



An extension of the logistic function to account for nonstationary drought losses

Tongtiegang Zhao¹, Zecong Chen¹, Yongyong Zhang², Bingyao Zhang³, and Yu Li³

¹Southern Marine Science and Engineering Guangdong Laboratory (Zhuhai), School of Civil Engineering, Sun Yat-sen University, Guangzhou 510275, China

²Key Laboratory of Water Cycle and Related Land Surface Processes, Institute of Geographic Sciences and Natural Resources Research, Chinese Academy of Sciences, Beijing 100101, China

³School of Hydraulic Engineering, Dalian University of Technology, Dalian 116024, China

Correspondence: Tongtiegang Zhao (zhaottg@mail.sysu.edu.cn) and Zecong Chen (chenzc8@mail2.sysu.edu.cn)

Received: 7 November 2024 – Discussion started: 28 November 2024

Revised: 6 February 2025 – Accepted: 12 March 2025 – Published: 11 June 2025

Abstract. While the stationary intensity loss function is fundamental to drought impact assessment, the relationship between drought loss and intensity can change as time progresses owing to socio-economic developments. This paper addresses this critical gap by modelling nonstationary drought losses. Specifically, time is explicitly formulated by linear and quadratic functions and then incorporated into the magnitude, shape and location parameters of the logistic function to derive six nonstationary intensity loss functions in total. To examine the effectiveness of this approach, a case study is designed for drought-affected populations by province in mainland China during the period from 2006 to 2023. The results highlight the existence of nonstationarity in that the drought-affected population exhibits significant correlation not only with the standard precipitation index but also with time. The proposed nonstationary intensity loss functions are shown to outperform not only the classic logistic function but also the linear regression. They present effective characterizations of observed drought loss in different ways: (1) the nonstationary function with the flexible magnitude parameter fits the data by adjusting the maximum drought loss by year; (2) the nonstationary function with the flexible shape parameter works by modifying the growth rate of drought loss with intensity; and (3) the nonstationary function with the flexible location parameter acts by shifting the response curves along the axis by year. Among the nonstationary logistic functions, the function incorporating the linear function of time into the magnitude parameter generally outperforms the others in terms of having a high coefficient

of determination, a low Bayesian information criterion and an explicit physical meaning. Taken together, the nonstationary intensity loss functions developed in this paper can serve as an effective tool for drought management.

1 Introduction

Droughts are one of the most destructive natural hazards (Baez-Villanueva et al., 2024; Van Dijk et al., 2013; Zhang et al., 2022). In general, there exist meteorological, hydrological, agricultural and socio-economic droughts (Mishra and Singh, 2010). Originating from precipitation deficits and high atmospheric evaporative demands, droughts propagate through hydrological processes and eventually impair human beings and natural ecosystems (Gao et al., 2024a; Liu et al., 2024; Zhao et al., 2024a). From 2001 to 2009, the Millennium Drought in southeastern Australia amplified median rainfall reduction by up to 4 times in streamflow and reduced irrigated rice and cotton production by 99 % and 84 % respectively (Van Dijk et al., 2013). The 2012 summertime drought struck the Central Great Plains in North America without early warning and caused more than USD 30 billion in economic losses (Hoerling et al., 2014; Yuan et al., 2023). The 2021/2022 drought event placed 76.2 % of the Euro-Mediterranean region under mild drought, 61.4 % under moderate drought and 39.4 % under severe drought (Garrido-Perez et al., 2024). Under climate change, droughts

are expected to not only increase worldwide (Dai, 2011) but also intensify more rapidly (Yuan et al., 2023).

Socio-economic losses are an integral part of droughts in environmental management (AghaKouchak et al., 2021; Hoerling et al., 2014; Van Dijk et al., 2013). Although there exist extensive studies on hydroclimatic processes associated with droughts (Entekhabi, 2023; Mishra and Singh, 2010; Wang et al., 2023b; Yang et al., 2024; Zhang et al., 2021), far less attention has been paid to the socio-economic impacts of droughts (AghaKouchak et al., 2021; Apurv and Cai, 2021; Su et al., 2018). One possible cause is the lack of socio-economic data on droughts (Su et al., 2018; Yang et al., 2024). On the one hand, in situ observations, satellite remote sensing and Earth system models generate a vast amount of hydroclimatic data (Hersbach et al., 2020; Pradhan et al., 2022; Zhang et al., 2024, 2021; Zhao et al., 2024b). Plenty of spatial–temporal data facilitates drought investigations at catchment, regional, continental and global scales and on pentad, monthly, seasonal and annual time steps (Gao et al., 2024b; Ma et al., 2022; Wang et al., 2023a). On the other hand, there are limited data on socio-economic losses due to droughts (AghaKouchak et al., 2021). Usually, drought losses have to be collected from statistical yearbooks issued by local and central governments and from survey reports provided by international organizations and commercial services (Chen et al., 2015; Hou et al., 2019).

The intensity loss function, which is also described as the exposure–response curve and dose–response relationship, plays a critical part in disaster risk management (AghaKouchak et al., 2021; Qiu et al., 2023; West et al., 2019). The classic logistic function is effective in characterizing the growth of socio-economic loss with drought intensity (Chen et al., 2015; Hou et al., 2019; Todisco et al., 2013). Moreover, the relationship between socio-economic loss and drought intensity can be nonstationary, i.e. temporally changing, considering that economic growth can increase exposure to droughts and that infrastructure developments can increase resilience to droughts (Apurv and Cai, 2021; Haile et al., 2020; Long et al., 2020). In this paper, we build three nonstationary functions upon the magnitude, shape and location parameters of the classic logistic function that represents a stationary intensity loss function. As is illustrated in the methods and results, the proposed functions tend to capture the nonstationary characteristics of drought-affected populations in mainland China. The effects of drought intensity and time on populations in different provinces are effectively characterized.

2 Methods

2.1 Intensity loss function

Drought indices are essential for drought impact assessment (Montanari et al., 2023; Todisco et al., 2013; West

et al., 2019). Among the popular indices are the standardized precipitation index (SPI), the Palmer drought severity index (PDSI), the standardized precipitation evapotranspiration index (SPEI) and the standardized runoff index (SRI) (AghaKouchak et al., 2021; Apurv and Cai, 2021; Zhao et al., 2024b). The intensity is derived from drought indices (Hao et al., 2017; Mishra and Singh, 2010; Su et al., 2018). As 0 is both the mean and the median values of the standard normal distribution, the extent to which drought indices fall below 0 indicates the degree of dryness. Thresholds can be employed to identify drought events (Wang et al., 2023b). For example, $(-0.99, 0]$ is near normal, $(-1.49, -1.00]$ is moderately dry, $(-1.99, -1.50]$ is severely dry and $(-\infty, -2.00]$ is extremely dry. Therefore, drought events can be defined by a combination of multiple indices, e.g. by $\text{SPI} \leq -1.0$, $\text{PDSI} \leq -2.0$ and $\text{SPEI} \leq -1.0$ (Su et al., 2018).

Denoting the drought intensity as I , the intensity loss function is formulated as

$$L = f(I), \quad (1)$$

in which L is the drought loss corresponding to the intensity I . Empirically, there are four important characteristics of $f(I)$: (1) there is minimal loss when there is minimal I ; (2) there is maximal loss when there is maximal I ; (3) $f(I)$ is a monotonically increasing function (i.e. drought loss increases with drought intensity); and (4) drought loss grows slowly with I initially, rises rapidly as I increases and then slows down until maturity.

The above four characteristics can mathematically be formulated by the renowned logistic function (Chen et al., 2015; Jonkman et al., 2008; Kucharavy and De Guio, 2011):

$$L(I) = \frac{A}{1 + e^{-k(I-c)}}, \quad (2)$$

in which there are three parameters, namely (1) the magnitude parameter A representing the maximum drought loss, (2) the shape parameter k controlling the growth rate of L with I and (3) the location parameter c indicating the point at which the saturation begins.

Drought indices that represent intensity can be derived from the target hydroclimatic variable's cumulative distribution function (CDF) and the inverse CDF of the standard normal distribution (Hao et al., 2017; Mishra and Singh, 2010; Montanari et al., 2023; Zhang et al., 2024; Zhao et al., 2024b). For example, SPI is calculated as

$$\text{SPI}_t = \text{CDF}_{N(0,1)}^{-1}(\text{CDF}_p(p_t)), \quad (3)$$

in which SPI_t in period t , which follows the standard normal distribution, is derived from precipitation amount p_t in period t . There are two steps: firstly, p_t is converted into a standard uniform variate between 0 and 1 by its CDF, i.e. $\text{CDF}_p(\cdot)$, and secondly, the standard uniform variate is converted into the standard normal variate SPI_t by the inverse CDF of $N(0,1^2)$, i.e. $\text{CDF}_{N(0,1)}^{-1}(\cdot)$. Similarly, SPEI is derived

from the difference between precipitation and potential evapotranspiration (Baez-Villanueva et al., 2024). Furthermore, the self-calibrating PDSI (scPDSI) takes into account evapotranspiration, recharge, runoff and loss in order to report dry conditions with frequencies that would be expected for rare conditions (Wells et al., 2004).

2.2 Formulation of the logistic function

There is an inverse relationship between drought intensity and drought indices such as SPI, SPEI and scPDSI. It is because the extent of dryness is generally characterized by how negative drought indices are (Haile et al., 2020; Liu et al., 2024; Zhang et al., 2021). That is, the more intense the dryness, the more negative the drought indices. Taking SPI as an indicator of drought intensity, the logistic function is modified by removing the negative sign in front of k :

$$L(\text{SPI}) = \frac{A}{1 + e^{k(\text{SPI}-c)}} \quad (4)$$

The ranges of the three parameters can be predetermined in accordance with the physical meanings of the parameters. First of all,

$$A > 0, \quad (5)$$

which means that drought loss is always above 0.

Second,

$$k > 0, \quad (6)$$

which means that as the SPI increases from $-\infty$ to $+\infty$, the denominator in Eq. (6) increases and leads to a reduction in drought loss. Eventually, the increasing denominator causes drought loss to approach 0 when SPI is large enough. On the other hand, it is noted that the loss begins to increase with SPI when k is negative.

Third,

$$-\infty < c < +\infty, \quad (7)$$

which means that the value of c depends on the case under investigation and can change freely.

An illustrative example of the logistic function in Eq. (4) is presented in Fig. 1. The result under the basic parameter set of ($A = 1.0, k = 5.0, c = 0.0$) is marked in black. There are three one-factor-at-a-time experiments (Chen and Zhao, 2020). First, the value of A is increased to 1.5. As is shown by the red line, the maximum drought loss evidently increases, but the shape of the line stays the same. Second, the value of k is reduced to 3.0. As is shown by the green line, the shape of the line becomes flatter, but the maximum loss remains the same. Third, the value of c is decreased to -1.0 . As is shown by the blue line, the curve is shifted to the left as a whole, while both the maximum loss and the shape do not change.

2.3 Stationary and nonstationary formulations

There are socio-economic factors that contribute to temporal changes, i.e. nonstationarity, in the intensity loss function (AghaKouchak et al., 2021; Chiang et al., 2021; Long et al., 2020). First, exposure to drought can increase with time owing to population growth, wealth accumulation and infrastructure development. Second, vulnerability under a given level of drought intensity may decrease with time considering engineering measures, such as the construction of water storage reservoirs and inter-basin water diversion projects. Third, resilience to drought can be improved by drought management measures, such as sub-seasonal to seasonal hydroclimatic forecasting and forecast-informed reservoir operation. In general, the relationship between drought loss and intensity tends to evolve as time progresses due to socio-economic developments and deployment of engineering and non-engineering drought-coping strategies (Hou et al., 2019; Jonkman et al., 2008; Su et al., 2018).

Without considering temporal changes, there is a stationary logistic function $L_{A0k0c0}(\cdot)$:

$$L_{A0k0c0}(\text{SPI}_t) = \frac{A_0}{1 + e^{k_0(\text{SPI}_t - c_0)}} \quad (8)$$

To account for temporal change, the linear function that takes time t as an explanatory variable (Cheng et al., 2014; Xiong et al., 2015) can be formulated for the parameters A, k and c :

$$\begin{cases} A_t = A_0 + A_1 \times t \\ k_t = k_0 + k_1 \times t \\ c_t = c_0 + c_1 \times t \end{cases}, \quad (9)$$

in which A_0, k_0 and c_0 are the intercepts, while A_1, k_1 and c_1 are the slopes. The incorporation of Eq. (9) into Eq. (8) yields the following three equations:

$$\begin{cases} L_{A1k0c0}(\text{SPI}_t) = \frac{A_0 + A_1 \times t}{1 + e^{k_0(\text{SPI}_t - c_0)}} \\ L_{A0k1c0}(\text{SPI}_t) = \frac{A_0}{1 + e^{(k_0 + k_1 \times t) \times (\text{SPI}_t - c_0)}} \\ L_{A0k0c1}(\text{SPI}_t) = \frac{A_0}{1 + e^{k_0(\text{SPI}_t - (c_0 + c_1 \times t))}} \end{cases}, \quad (10)$$

in which the logistic functions $L_{A1k0c0}(\text{SPI}_t), L_{A0k1c0}(\text{SPI}_t)$ and $L_{A0k0c1}(\text{SPI}_t)$ have nonstationary magnitude, shape and location parameters respectively.

Furthermore, the quadratic function can be used to accommodate possibly nonlinear changes:

$$\begin{cases} A_t = A_0 + A_1 \times t + A_2 \times t^2 \\ k_t = k_0 + k_1 \times t + k_2 \times t^2 \\ c_t = c_0 + c_1 \times t + c_2 \times t^2 \end{cases}. \quad (11)$$

The incorporation of Eq. (11) into Eq. (8) yields another three equations:

$$\begin{cases} L_{A2k0c0}(\text{SPI}_t) = \frac{A_0 + A_1 \times t + A_2 \times t^2}{1 + e^{k_0(\text{SPI}_t - c_0)}} \\ L_{A0k2c0}(\text{SPI}_t) = \frac{A_0}{1 + e^{(k_0 + k_1 \times t + k_2 \times t^2) \times (\text{SPI}_t - c_0)}} \\ L_{A0k0c2}(\text{SPI}_t) = \frac{A_0}{1 + e^{k_0(\text{SPI}_t - (c_0 + c_1 \times t + c_2 \times t^2))}} \end{cases}. \quad (12)$$

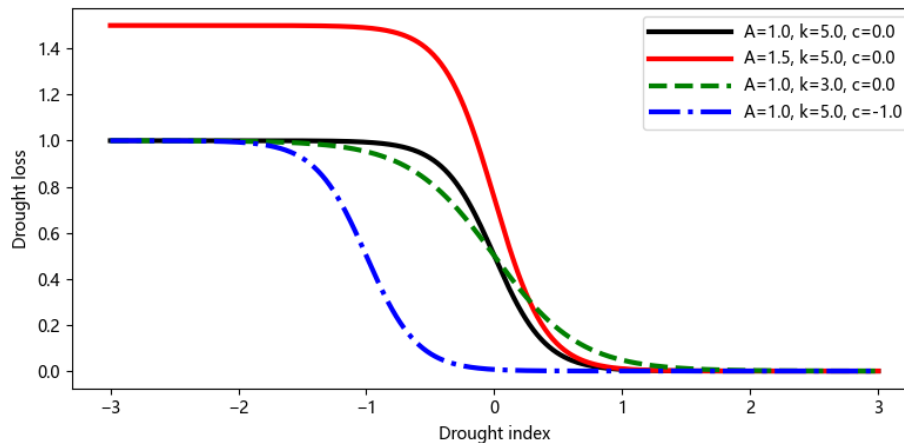


Figure 1. An illustrative example of the logistic function under four sets of parameters.

In Eqs. (8), (10) and (12), the subscripts “ Ax ”, “ kx ” and “ cx ” denote the magnitude, shape and location parameters respectively. For “ x ”, the values 0, 1 and 2 indicate the non-involvement of time, the linear function of time and the quadratic function of time respectively. As a result, the logistic function is nonstationary when x is 1 or 2. For example, $L_{A1k0c0}(SPI_t)$ represents the nonstationary logistic function involving the linear function of time for the magnitude parameter.

Fitting the stationary and nonstationary functions is considered to be a nonlinear least-squares problem by searching for the set of parameters that minimizes the sum of the squares of residuals. It is performed using the `curve_fit` function in the SciPy optimization toolbox (Virtanen et al., 2020).

3 Case study

3.1 Data description

The drought loss data are sourced from the Ministry of Water Resources (MWR) of China. The MWR has published the Bulletin of Flood and Drought Disaster in China annually since 2006. The name of the bulletin was changed to the China Flood and Drought Disaster Prevention Bulletin in 2019. By collating floods and droughts reported by provincial governments and river basin commissions, the MWR has presented major events of droughts and floods across the 31 provinces in mainland China in its bulletin. With respect to droughts and floods in each province, the bulletin provides an annual account of quantitative socio-economic losses, contingency plans, and retrospective analyses of prevention and control measures.

Attention is paid to drought-affected populations, which represents the number of individuals suffering from the impacts of droughts as recorded in official reports. Figure 2 shows the multi-annual mean drought-affected population, maximum annual drought-affected population, mean annual

precipitation and total population. From Fig. 2a and b, it can be observed that provinces in southwestern China, including Yunnan, Guizhou and Sichuan, tend to have the largest population affected by droughts. In 2010 in particular, 9.65 million people in Yunnan Province and 7.57 million people in Guizhou Province were struck by a record-breaking drought event induced by the persistently positive Madden–Julian Oscillation (Lü et al., 2012). On the other hand, it can be seen from Fig. 2c and d that there is neither low precipitation nor a large population in southwestern China. In general, the large drought-affected population in Yunnan and Sichuan is attributed to the karst landscape, which is characterized by low storage capacity, high infiltration rate and fast groundwater flow (Wan et al., 2016).

The precipitation data used for the calculation of SPI are obtained from the Climate Hazards Group InfraRed Precipitation with Station data (CHIRPS) (Funk et al., 2015). The intersection operation is performed to use provincial polygons to extract spatially averaged precipitation from the CHIRPS raster precipitation field. To better characterize the climatological distribution of precipitation, time series of annual precipitation are extracted by province for the period from 1981 to 2023. The 43-year annual precipitation is first converted into CDF by Weibull’s plotting position (Ye et al., 2018) and then converted into SPI by the inverse CDF of $N(0,1^2)$. Then, SPI in the years from 2006 to 2023 is used in the fitting of the logistic functions.

Alongside the SPI data, the SPEI data are obtained from SPEIbase (Beguería et al., 2024). Specifically, SPEI-12 in December is selected to represent the annual drought condition as the loss is at the annual timescale, and the intersection operation is performed to use provincial polygons to extract the spatially averaged SPEI. Furthermore, scPDSI is sourced from the Climate Research Unit (CRU) (Barichivich et al., 2024). As scPDSI is monthly, the values across the 12 months within a year are averaged before taking the spatial average of each province.

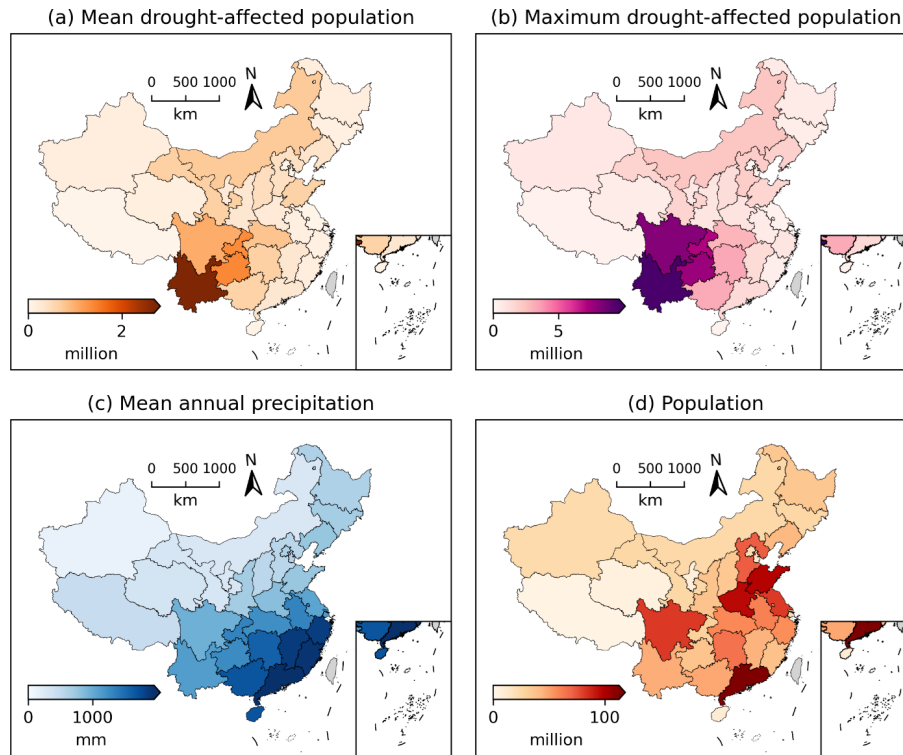


Figure 2. Spatial plots of (a) mean annual drought-affected population, (b) maximum annual drought-affected population, (c) mean annual precipitation and (d) population by province in mainland China. Publisher’s remark: please note that the above figure contains disputed territories.

3.2 Model evaluation

The coefficient of determination, i.e. R^2 , is evaluated for the stationary logistic function (Eq. 8) and the six types of nonstationary logistic functions (Eqs. 10 and 12). That is, the sum of squares of residuals for the estimations provided by the functions is compared to the baseline sum of squares of residuals for the mean value. As a result, R^2 represents the ratio of total variation in the drought loss that is explained as follows:

$$R^2 = 1 - \frac{\sum_t (L_t - \hat{L}_t)^2}{\sum_t (L_t - \bar{L})^2}, \tag{13}$$

in which L_t is the drought loss in year t , \hat{L}_t is the loss estimated by the function under investigation and \bar{L} is the mean value of all L_t values.

The number of parameters plays a critical part in statistical modelling. That is, more parameters facilitate more flexible fitting of observed data but are also more prone to overfitting (Neath and Cavanaugh, 2012). There are three parameters for the stationary logistic function, four parameters for the nonstationary logistic functions with the linear function and five parameters for the nonstationary logistic functions with

the quadratic function:

$$\begin{cases} n_{A0k0c0} = 3 \\ n_{A1k0c0} = 4 \\ n_{A0k1c1} = 4 \\ n_{A0k0c1} = 4 \\ n_{A2k0c0} = 5 \\ n_{A0k2c0} = 5 \\ n_{A0k0c2} = 5 \end{cases} . \tag{14}$$

The Bayesian information criterion (BIC) takes into account both the sum of squares of residuals and the number of parameters (Neath and Cavanaugh, 2012):

$$BIC = T \times \ln \left(\frac{\sum_t (L_t - \hat{L}_t)^2}{T} \right) + n \times \ln(T), \tag{15}$$

in which $\ln(\cdot)$ is the natural logarithmic function, T is the number of observations and n is the number of parameters. BIC is negatively oriented, meaning that a lower value indicates a better fit. As a result, both a larger sum of squares of residuals and more parameters are penalized by the BIC.

4 Results

4.1 Correlation analysis

Pearson's correlation coefficients between the drought-affected population and time and between the drought-affected population and SPI are illustrated by bar plots in Fig. 3. There are a total of 31 provincial administrative regions in mainland China. Beijing, Tianjin, Shanghai and Xizang are not considered since they are excluded from the drought-affected population in most years. This outcome is mainly due to ample water availability and water supply facilities (Long et al., 2020; Sun et al., 2021). For the other 27 provincial administrative regions, it can be observed from Fig. 3a that the correlation coefficient between the drought-affected population and time is mostly significantly negative, while it is slightly positive in Guangdong and Fujian, although not significant. The implication is that the drought-affected population mostly exhibits a decreasing trend as time progresses and sometimes shows an increasing trend. From Fig. 3b, it is seen that the correlation coefficient between the drought-affected population and SPI is generally significantly negative. This result suggests that the drought-affected population tends to decrease as the amount of precipitation increases. Overall, the correlation coefficients in Fig. 3 point out that it is reasonable to use both time and SPI as explanatory variables of the drought-affected population.

The drought-affected population is plotted against time and SPI for Yunnan Province in Fig. 4 due to its remarkable mean annual drought-affected population (Wan et al., 2016) and for Guangdong Province in Fig. 5 due to its economic importance (Shao et al., 2020). The scatter plots on the left-hand side of the two figures imply the complexity of drought impact assessment. That is, owing to socio-economic developments, the drought-affected population can decrease or increase as time progresses (Apurv and Cai, 2021; Haile et al., 2020; Long et al., 2020). The scatter plots on the right-hand side suggest that the increase in precipitation effectively reduces the population affected by droughts (AghaKouchak et al., 2021; Qiu et al., 2023; West et al., 2019).

4.2 Decreasing drought-affected population

The stationary logistic function directly relates the drought-affected population to SPI (Fig. 6), while the nonstationary logistic functions account for the dependency of the drought-affected population on both SPI and time (Figs. 7 and 8).

In Fig. 6, it is shown that the mean drought-affected population is about 4 million, whereas the maximum reached 10 million in the year 2010. Furthermore, the data point with the maximum drought-affected population corresponds to SPI that is around 0, which is due to the fact that drought conditions depend not only on precipitation, but also on evapotranspiration, water storage and other hydroclimatic factors (Su et al., 2018; Yin et al., 2022a, b). In general, it is hard for

the stationary logistic function $A0k0c0$ to capture the data points with a lower SPI but a higher drought-affected population.

In Fig. 7, the nonstationary logistic functions $A1k0c0$, $A0k1c0$ and $A0k0c1$ are visualized by the surface and wireframe plots. While the correlation between the drought-affected population and time tends to be negative in Yunnan Province, it is observed that the nonstationary functions tend to capture not only the decrease in the drought-affected population with SPI, but also the decrease in the drought-affected population with time. Since the year with the maximum drought-affected population is in the early part of the study period, there is a remarkable increase in R^2 . The three functions perform differently in capturing the observed data points.

1. The flexible magnitude parameter in $A1k0c0$ tends to fit the observed data by reducing the maximum drought loss by year (Fig. 6a). As can be seen from the wireframe plot, the maximum drought loss evidently reduces from 2006 to 2023, while the shape and location of the curves remain the same.
2. The flexible shape parameter in $A0k1c0$ fits the observed data by changing the response surface, as shown in Fig. 6b. Although it exhibits the highest R^2 and the lowest BIC, the fitted drought-affected population is shown to counterintuitively increase with SPI in 2021, 2022 and 2023. That is, more people could be subject to drought as precipitation increases in these 3 years. This wrong outcome is because of the flexibility of the shape parameter. Specifically, the value of the shape parameter can be forced by the trend term to turn from positive to negative as time progresses. When the shape parameter is negative, the estimated drought impact increases with the precipitation amount.
3. The flexible location parameter in $A0k0c1$ tends to fit the observation data by shifting the response curves by year, as shown in Fig. 6c. Due to the fact that the maximum drought-affected population is fixed from 2006 to 2023, it is observed that the maximum affected population in 2010 is not effectively captured.

In Fig. 8, the nonstationary logistic functions $A2k0c0$, $A0k2c0$ and $A0k0c2$ are also visualized by the surface and wireframe plots. Although the quadratic function leads to some improvements in R^2 , the improvements are at the cost of the physical meaning of the results. From Fig. 8a, it is observed that under a given SPI that is below 0, the drought-affected population initially increases but then decreases with time. From Fig. 8b, it is observed that the response surface exhibits a complex shape that can be due to the fitting of sample-specific noise. The implication is that the data points are too limited to facilitate the fitting of a quadratic function in $A2k0c0$, $A0k2c0$ and $A0k0c2$.

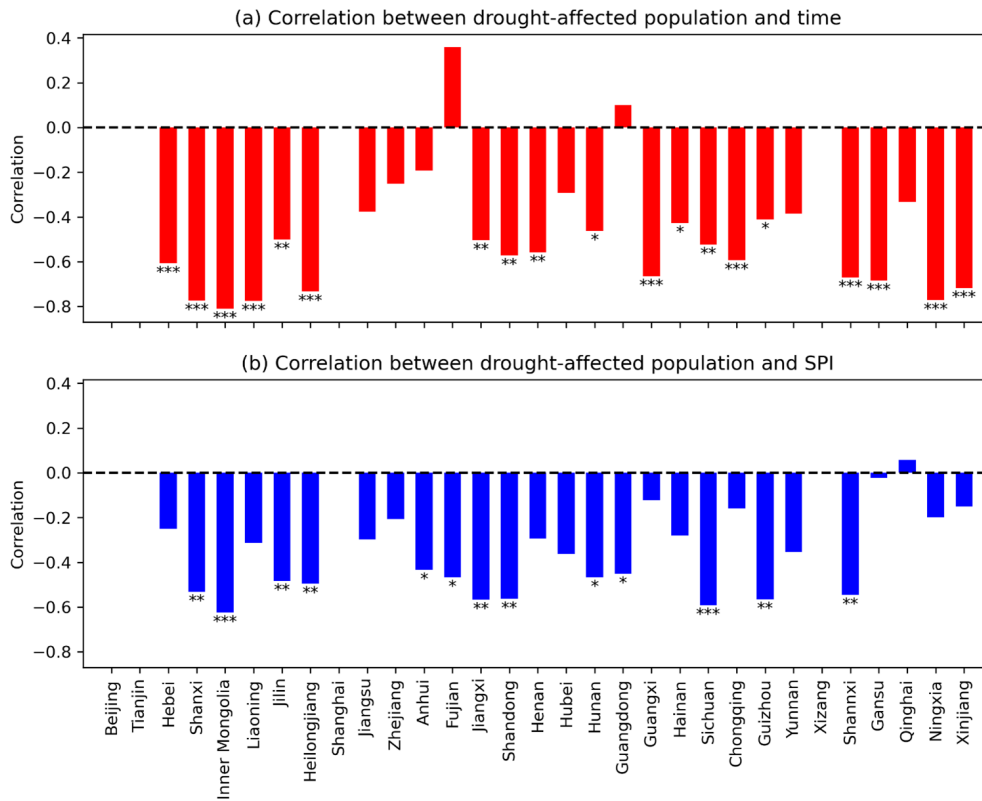


Figure 3. Correlation coefficient between the drought-affected population and (a) time and between the drought-affected population and (b) SPI by province. Alongside the bars are *, ** and ***, indicating the significance at the levels of 0.10, 0.05 and 0.01 respectively. Bars without * imply non-significant correlation coefficients.

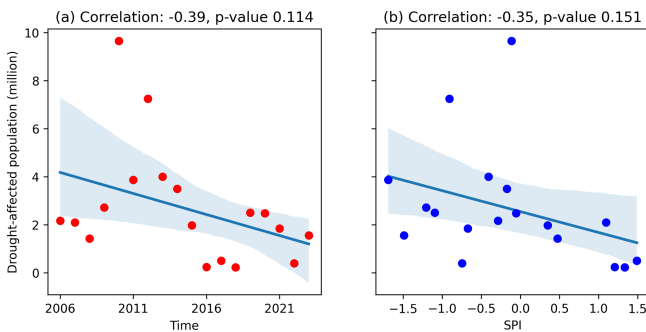


Figure 4. Scatter plots of the drought-affected population against (a) time and (b) SPI in Yunnan Province.

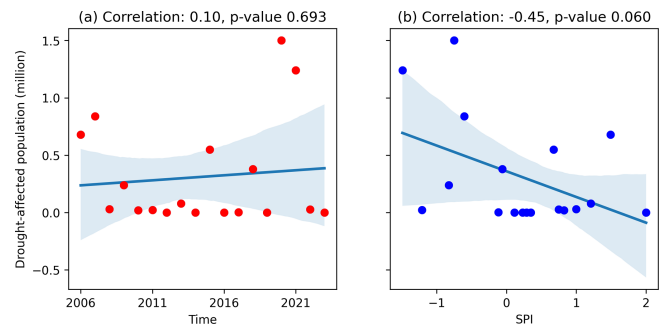


Figure 5. As for Fig. 4 but for Guangdong Province.

4.3 Increasing drought-affected population

The stationary and nonstationary logistic functions are furthermore applied to Guangdong Province (Shao et al., 2020). Since the population of Guangdong is concentrated on the Pearl River Delta, recent years have witnessed a serious water scarcity due to upstream reservoir impoundments and estuary saltwater intrusion (Weng et al., 2024).

From Fig. 9, it is observed that there can be a considerable drought-affected population when the precipitation is

above average. The stationary logistic function $A0k0c0$ tends to capture the decrease in drought-affected population with SPI. However, it is difficult for this function to capture data points with large drought-affected populations.

From Fig. 10, it is seen that the three nonstationary logistic functions, $A1k0c0$, $A0k1c0$ and $A0k0c1$, are more effective in characterizing the dependency of the drought-affected population on SPI and time. The linear function plays different parts in these three functions.

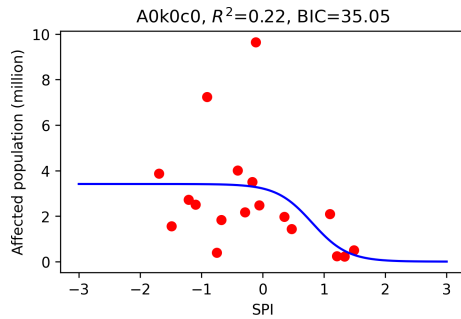


Figure 6. Illustration of the stationary logistic function A0k0c0 fitting the relationship between SPI and the drought-affected population for Yunnan Province.

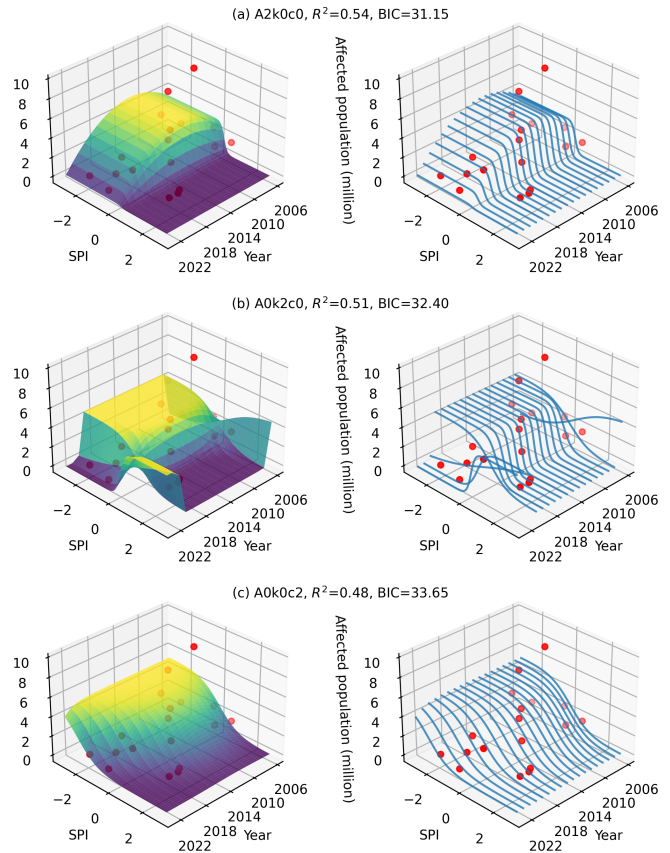


Figure 8. As for Fig. 7 but for the nonstationary logistic functions (a) A2k0c0, (b) A0k2c0 and (c) A0k0c2.

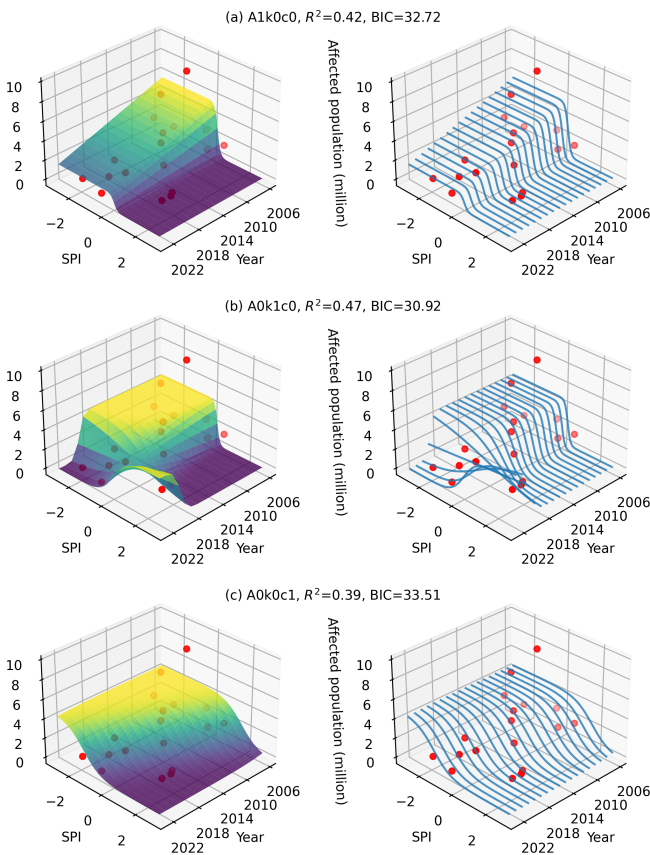


Figure 7. Surface plots (left) and wireframe plots (right) for the nonstationary logistic functions (a) A1k0c0, (b) A0k1c0 and (c) A0k0c1, relating the drought-affected population to SPI and time for Yunnan Province.

1. The linear magnitude parameter in A1k0c0 tends to fit the increase by enlarging the maximum drought loss by year. As shown in Fig. 10a, it tends to capture the maximum drought-affected population of 1.50 million in 2020 and the second maximum drought-affected population of 1.24 million in 2021.

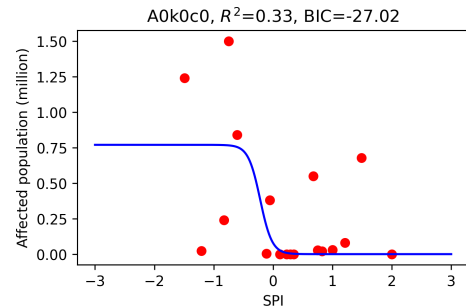


Figure 9. Illustration of the stationary logistic function A0k0c0 fitting the relationship between SPI and drought-affected populations for Guangdong Province.

2. The linear shape parameter in A0k1c0 is observed to fit the observation data by changing the shape of the response surface by year. As shown in Fig. 10b, although the affected population in 2020 and 2021 is characterized to some extent, the drought-affected population is seen to increase unexpectedly with SPI in 2006. These results highlight the role that the shape parameter plays in determining the growth (reduction) rate.

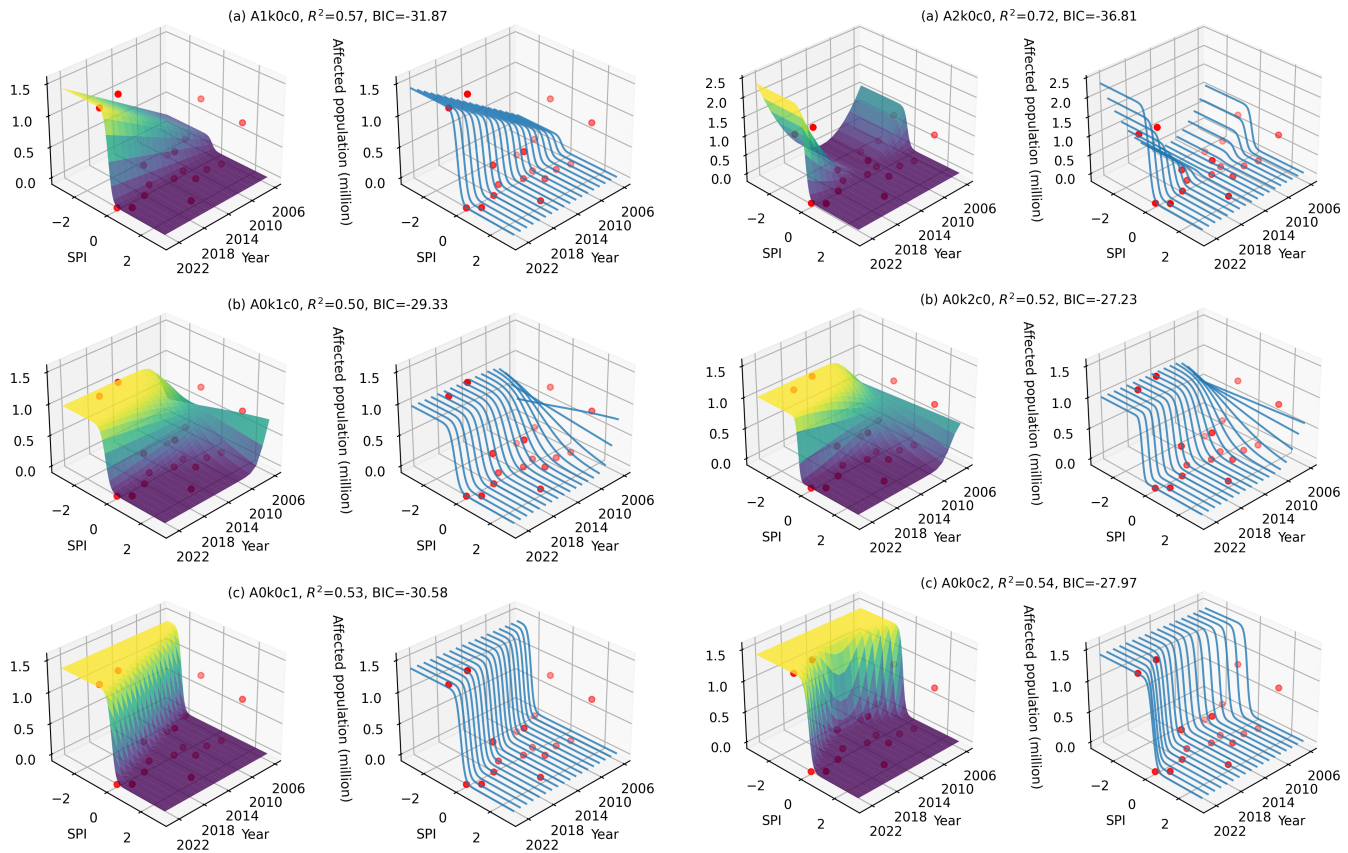


Figure 10. Surface plots (left) and wireframe plots (right) for the nonstationary logistic functions (a) A1k0c0, (b) A0k1c0 and (c) A0k0c1, relating the drought-affected population to SPI and time for Guangdong Province.

Figure 11. As for Fig. 10 but for the nonstationary logistic functions (a) A2k0c0, (b) A0k2c0 and (c) A0k0c2.

3. The linear location parameter in A0k0c1 is shown to fit the observation data by fixing the maximum drought loss but shifting the response curves by year. As shown in Fig. 10c, it tends to characterize the maximum and second maximum drought-affected population in recent years but does not seem to be as effective in characterizing the drought-affected population in early years.

From Fig. 11, it is observed that the three nonstationary logistic functions, A2k0c0, A0k2c0 and A0k0c2, also tend to capture the drought-affected population. The result in Fig. 11a is generally hard to interpret since the drought-affected population tends to initially decrease but then increase with time under a given SPI below 0. The results in Fig. 11b and c are similar to those in Fig. 10b and c respectively. The implication is that the linear function in A0k1c0 and A0k0c1 can be as effective as the quadratic function in A0k2c0 and A0k0c2.

4.4 Goodness of fit

The stationary and nonstationary logistic functions are set up to account for the drought-affected population based on the explanatory variables of time and SPI for 27 provincial administrative regions other than Beijing, Tianjin, Shanghai and Xizang. The R^2 for the three nonstationary logistic functions, A1k0c0, A0k1c0 and A0k0c1, are plotted against that of linear regression based on time (Fig. 12a) and also against that of the stationary logistic function (Fig. 12b). The three scatter plots are generally above the 1 : 1 line. This result indicates that the consideration of time t evidently enhances the proportion of total variation explained by the nonstationary logistic functions. It is noted that the mean R^2 is 0.307 for linear regression and 0.269 for the stationary logistic function A0k0c0. By contrast, the mean R^2 is 0.512, 0.506 and 0.509 for A1k0c0, A0k1c0 and A0k0c1 respectively. Overall, the nonstationary logistic function A1k0c0 has the highest R^2 . This result highlights that the incorporation of time into the magnitude parameter can effectively deal with the nonstationary drought-affected population. Furthermore, the R^2 of A2k0c0, A0k2c0 and A0k0c2 is investigated in Fig. S15 of the Supplement. The results highlight the improvements in R^2 for the nonstationary logistic functions.

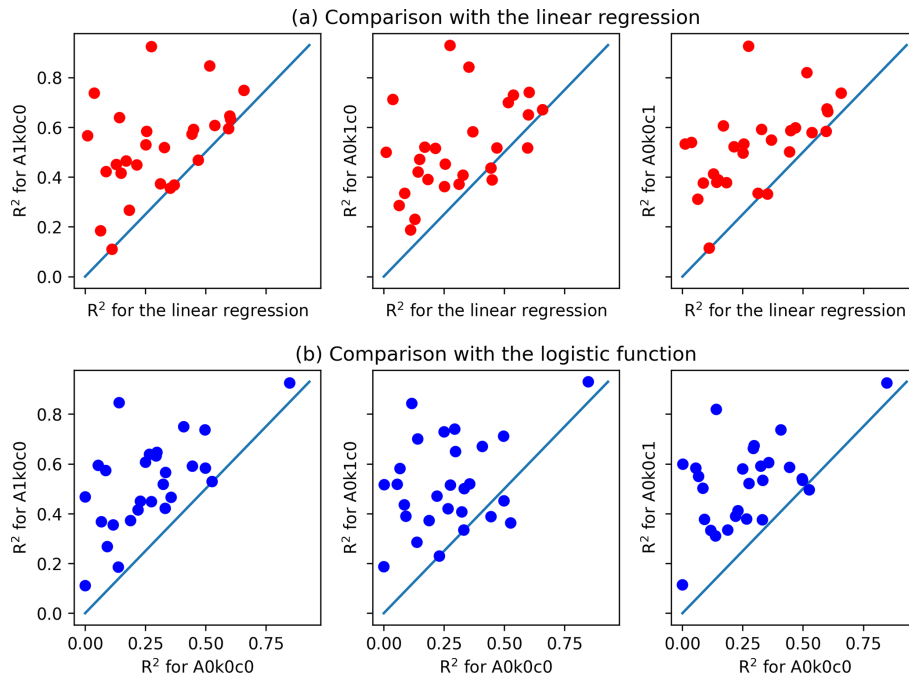


Figure 12. Scatter plots of the R^2 for the three nonstationary logistic functions against the R^2 for (a) the linear regression and (b) the stationary logistic function A0k0c0.

Furthermore, the BIC of the three nonstationary logistic functions, A1k0c0, A0k1c0 and A0k0c1, is plotted against the BIC of the linear regression in Fig. 13a and against that of the stationary logistic function in Fig. 13b. Since the higher R^2 of the nonstationary logistic functions in Fig. 12 is at the cost of an additional parameter (Neath and Cavanaugh, 2012), the BIC takes into account not only the number of parameters but also the mean squared error. It can be observed that the scatter plots in Fig. 13 are largely below the 1 : 1 line. Considering that the BIC is a negatively oriented metric, this result suggests that there is a low risk of overfitting and that the information hidden in the significant correlation is deemed to be effectively exploited by the three nonstationary logistic functions. It is noted that the mean BIC is -33.105 for linear regression and -29.365 for the stationary logistic function A0k0c0. By contrast, the mean BIC is -34.980 , -34.772 and -34.740 for A1k0c0, A0k1c0 and A0k0c1 respectively. As the nonstationary logistic function A1k0c0 has the lowest BIC, it is highlighted that the incorporation of time into the magnitude parameter of the logistic function is effective in accounting for the nonstationarity of drought losses. Furthermore, the BIC of A2k0c0, A0k2c0 and A0k0c2 is investigated in Fig. S16. Overall, the results are similar to those in Fig. 13. The implication is that the incorporation of the linear function into the logistic function suffices to deal with the dependency of the drought-affected population on SPI and time.

5 Discussion

This paper has furthermore designed experiments to investigate the robustness of the nonstationary logistic functions using the drought indices SPEI and scPDSI (AghaKouchak et al., 2021; Apurv and Cai, 2021; Zhao et al., 2024b). The additional results are presented in the supplementary material. Specifically, as for SPEI, the correlation is presented in Fig. S1, and the plots for Yunnan and Guangdong are provided in Figs. S2 to S7; as for scPDSI, the correlation is presented in Fig. S8, and the plots for Yunnan and Guangdong are shown in Figs. S9 to S14. Overall, the results under SPEI and scPDSI conform to those under SPI. While the nonstationarity plays an important part in the relationship between the drought-affected population and drought conditions, it is highlighted that the nonstationary logistic functions are effective in characterizing the dependency of the drought-affected population on drought conditions and time. It is also pointed out that different drought indices have varying efficiency in characterizing the drought conditions. For example, the lower R^2 in Fig. 6 is largely due to the correspondence of the maximum drought-affected population with average precipitation in the year 2010; R^2 evidently increases from 0.22 under SPI (Fig. 6) to 0.42 under SPEI (Fig. S2) and, furthermore, to 0.58 under scPDSI (Fig. S9). This result highlights that drought conditions depend on precipitation and also on other hydroclimatic variables, such as evapotranspiration, recharge and runoff (Wells et al., 2004; Yin et al., 2022b).

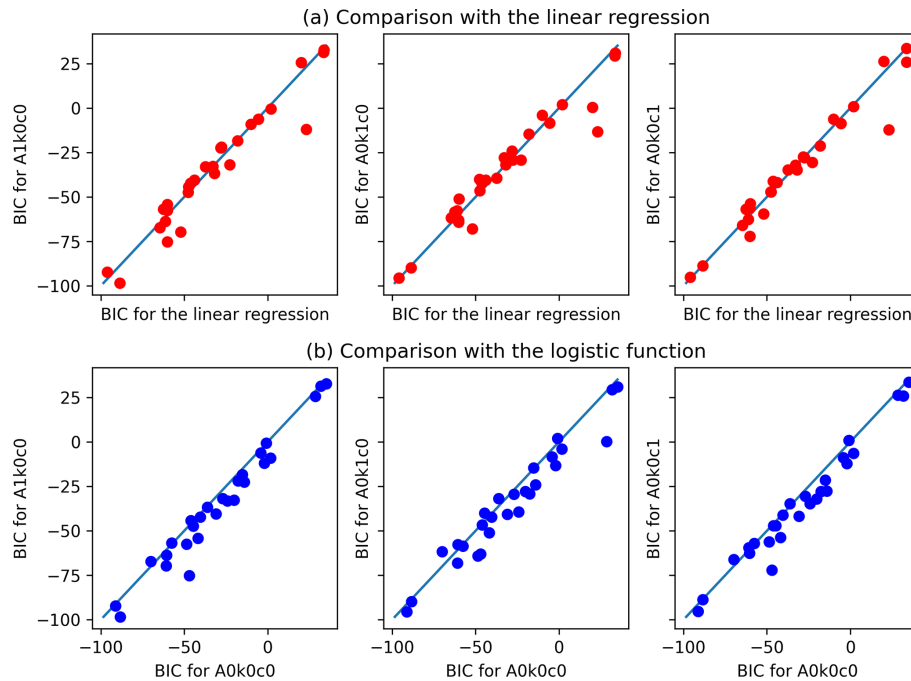


Figure 13. As for Fig. 12 but for the BIC.

The nonstationary intensity loss functions developed in this paper complement existing studies on hydroclimatic processes of droughts (Garrido-Perez et al., 2024; Haile et al., 2020; Todisco et al., 2013). The frequency, duration and intensity are three important characteristics of droughts (Baez-Villanueva et al., 2024; Entekhabi, 2023; Liu et al., 2024; Mishra and Singh, 2010; Yang et al., 2024). Given a threshold for the identification of drought events, frequency is generally defined as the number of drought events in a certain period (1 year for example), duration as the time span of a drought event and intensity as the cumulative sum of the drought index (AghaKouchak et al., 2021; Chiang et al., 2021). Given that SPI is derived for annual precipitation in this paper, the SPI values are expected to reflect the conditions of drought frequency, duration and intensity across different years. It is noted that the use of annual precipitation is mainly due to the fact that the drought-affected population by province is available at the annual timescale. It is possible that drought losses are available on an event scale. In that case, event-based analysis becomes feasible. That is, both drought loss and intensity can be quantified for each drought event, and the effectiveness of the logistic function can then be tested.

Focusing on drought indices such as SPI, PDSI, SPEI and SRI, previous studies have presented in-depth investigations into past changes and future projections of meteorological, hydrological, agricultural and socio-economic droughts (Apurv and Cai, 2021; Hao and Singh, 2015; Mishra and Singh, 2010). Under climate change, droughts are increasingly found to be interconnected with other extreme events,

including heatwaves (Yin et al., 2022a), tropical cyclones (Gao et al., 2024c), drought–flood abrupt alternation (Shi et al., 2021) and summer drought–flood coexistence (Wu et al., 2006). This paper proposes the inclusion of time as a covariate to capture the overall trend of nonstationary drought losses. One remarkable feature of the proposed intensity loss function is the explicit estimation of drought loss under different combinations of drought indices and times. As the frequency and intensity of these compound disasters continue to increase, socio-economic losses are expected to rise in the future. The relationship between socio-economic losses and other disaster indices can readily be investigated at local and regional scales. Given that the logistic function is already an established growth model in biosciences (Tsoularis and Wallace, 2002), it is expected that the proposed functions can be used to characterize the growth of drought loss with drought conditions characterized by different drought indices.

6 Conclusions

This paper has presented nonstationary intensity loss functions for drought impact assessment. On the one hand, the classic logistic function that has three parameters, i.e. magnitude, shape and location, presents a stationary formulation of the growth of drought losses with drought conditions. On the other hand, the incorporations of time as linear and quadratic functions into the magnitude, shape and location parameters facilitate in total six nonstationary logistic functions. A case study is presented for the drought-affected population by

province in China during the period from 2006 to 2023. The results highlight that despite the fact that drought-affected populations can either decrease or increase with time, the joint use of both SPI and time as explanatory variables leads to effective characterization of drought-affected populations. In comparison with the stationary logistic function, the effectiveness of the nonstationary logistic functions is indicated not only by higher R^2 , which indicates a reasonable proportion of total explained variation, but also by lower BIC, which suggests low risk of overfitting. Among the nonstationary logistic functions, the function incorporating the linear function of time into the magnitude parameter generally outperforms the others in terms of higher R^2 , lower BIC and clearer physical meanings. In conclusion, the nonstationary intensity loss functions developed in this paper can improve our understanding of and response to drought risks in an era of rapid socio-economic and environmental change. Future research could further enhance this framework by incorporating additional socio-economic variables to refine the model's predictive capabilities and support targeted mitigation strategies.

Data availability. The drought-affected population is available from the Ministry of Water Resources of China. The CHIRPS precipitation data are available from the Climate Hazards Center at the University of California, Santa Barbara (<https://www.chc.ucsb.edu/data/chirps>, Funk et al., 2015). The SPEI data are available from the global SPEI database (<https://doi.org/10.20350/digitalCSIC/16497>, Beguería et al., 2024). The scPDSI data are available from the Climatic Research Unit (CRU) (<https://crudata.uea.ac.uk/cru/data/drought/>, Barichivich et al., 2024).

Supplement. The supplement related to this article is available online at <https://doi.org/10.5194/hess-29-2429-2025-supplement>.

Author contributions. TZ: writing – original draft, visualization, software, methodology, conceptualization. ZC: validation, resources, data curation. YZ: investigation, formal analysis. BZ: visualization, data curation. YL: validation, data curation.

Competing interests. The contact author has declared that none of the authors has any competing interests.

Disclaimer. Publisher's note: Copernicus Publications remains neutral with regard to jurisdictional claims made in the text, published maps, institutional affiliations, or any other geographical representation in this paper. While Copernicus Publications makes every effort to include appropriate place names, the final responsibility lies with the authors.

Acknowledgements. This research is supported by the National Natural Science Foundation of China (grant nos. 2023YFF0804900 and 52379033) and the Guangdong Provincial Department of Science and Technology (grant no. 2019ZT08G090).

Financial support. This research has been supported by the National Natural Science Foundation of China (grant nos. 2023YFF0804900 and 52379033) and the Guangdong Provincial Department of Science and Technology (grant no. 2019ZT08G090).

Review statement. This paper was edited by Xing Yuan and reviewed by two anonymous referees.

References

- AghaKouchak, A., Mirchi, A., Madani, K., Di Baldassarre, G., Nazemi, A., Alborzi, A., Anjileli, H., Azarderakhsh, M., Chiang, F., Hassanzadeh, E., Huning, L. S., Mallakpour, I., Martinez, A., Mazdiyasn, O., Moftakhari, H., Norouzi, H., Sadegh, M., Sadeqi, D., Van Loon, A. F., and Wanders, N.: Anthropogenic Drought: Definition, Challenges, and Opportunities, *Rev. Geophys.*, 59, e2019RG000683, <https://doi.org/10.1029/2019RG000683>, 2021.
- Apurv, T. and Cai, X.: Regional Drought Risk in the Contiguous United States, *Geophys. Res. Lett.*, 48, e2020GL092200, <https://doi.org/10.1029/2020GL092200>, 2021.
- Baez-Villanueva, O. M., Zambrano-Bigiarini, M., Miralles, D. G., Beck, H. E., Siegmund, J. F., Alvarez-Garreton, C., Verbist, K., Garreaud, R., Boisier, J. P., and Galleguillos, M.: On the timescale of drought indices for monitoring streamflow drought considering catchment hydrological regimes, *Hydrol. Earth Syst. Sci.*, 28, 1415–1439, <https://doi.org/10.5194/hess-28-1415-2024>, 2024.
- Barichivich, J., Osborn, T. J., Harris, I., van der Schrier, G., and Jones, P. D.: Monitoring global drought using the self-calibrating palmer drought severity index [in “state of the climate in 2023”], *B. Am. Meteorol. Soc.*, 105, S70–S71, <https://doi.org/10.1175/BAMS-D-24-0116.1>, 2024 (data available at: <https://crudata.uea.ac.uk/cru/data/drought/>, last access: 6 January 2025).
- Beguería, S., Vicente Serrano, S. M., Reig-Gracia, F., and Latorre Garcés, B.: SPEIbase v.2.10 [dataset]: A comprehensive tool for global drought analysis, Consejo Superior de Investigaciones Científicas [data set], <https://doi.org/10.20350/digitalCSIC/16497>, 2024.
- Chen, H. and Zhao, T.: Modeling power loss during blackouts in China using non-stationary generalized extreme value distribution, *Energy*, 195, 117044, <https://doi.org/10.1016/j.energy.2020.117044>, 2020.
- Chen, M., Ma, J., Hu, Y., Zhou, F., Li, J., and Yan, L.: Is the S-shaped curve a general law? An application to evaluate the damage resulting from water-induced disasters, *Nat. Hazards*, 78, 497–515, <https://doi.org/10.1007/s11069-015-1723-9>, 2015.
- Cheng, L., AghaKouchak, A., Gilleland, E., and Katz, R. W.: Non-stationary extreme value analysis in a changing climate,

- Climatic Change, 127, 353–369, <https://doi.org/10.1007/s10584-014-1254-5>, 2014.
- Chiang, F., Mazdiyasi, O., and AghaKouchak, A.: Evidence of anthropogenic impacts on global drought frequency, duration, and intensity, *Nat. Commun.*, 12, 2754, <https://doi.org/10.1038/s41467-021-22314-w>, 2021.
- Dai, A.: Drought under global warming: a review, *WIREs Clim. Change*, 2, 45–65, <https://doi.org/10.1002/wcc.81>, 2011.
- Entekhabi, D.: Propagation in the Drought Cascade: Observational Analysis Over the Continental US, *Water Resour. Res.*, 59, e2022WR032608, <https://doi.org/10.1029/2022WR032608>, 2023.
- Funk, C., Peterson, P., Landsfeld, M., Pedreros, D., Verdin, J., Shukla, S., Husak, G., Rowland, J., Harrison, L., Hoell, A., and Michaelsen, J.: The climate hazards infrared precipitation with stations – a new environmental record for monitoring extremes, *Scientific Data*, 2, 150066, <https://doi.org/10.1038/sdata.2015.66>, 2015 (data available at: <https://www.chc.ucsb.edu/data/chirps>, last access: 6 January 2025).
- Gao, H., Hrachowitz, M., Wang-Erlandsson, L., Fenicia, F., Xi, Q., Xia, J., Shao, W., Sun, G., and Savenije, H. H. G.: Root zone in the Earth system, *Hydrol. Earth Syst. Sci.*, 28, 4477–4499, <https://doi.org/10.5194/hess-28-4477-2024>, 2024a.
- Gao, Y., Zhao, T., Tu, T., Tian, Y., Zhang, Y., Liu, Z., Zheng, Y., Chen, X., and Wang, H.: Spatiotemporal links between meteorological and agricultural droughts impacted by tropical cyclones in China, *Sci. Total Environ.*, 912, 169119, <https://doi.org/10.1016/j.scitotenv.2023.169119>, 2024b.
- Gao, Y., Zhao, T., Tu, T., Tian, Y., Zhang, Y., Liu, Z., Zheng, Y., Chen, X., and Wang, H.: Spatiotemporal links between meteorological and agricultural droughts impacted by tropical cyclones in China, *Sci. Total Environ.*, 912, 169119, <https://doi.org/10.1016/j.scitotenv.2023.169119>, 2024c.
- Garrido-Perez, J. M., Vicente-Serrano, S. M., Barriopedro, D., García-Herrera, R., Trigo, R., and Beguería, S.: Examining the outstanding Euro-Mediterranean drought of 2021–2022 and its historical context, *J. Hydrol.*, 630, 130653, <https://doi.org/10.1016/j.jhydrol.2024.130653>, 2024.
- Haile, G. G., Tang, Q., Li, W., Liu, X., and Zhang, X.: Drought: Progress in broadening its understanding, *WIREs Water*, 7, e1407, <https://doi.org/10.1002/wat2.1407>, 2020.
- Hao, Z. and Singh, V. P.: Drought characterization from a multivariate perspective: A review, *J. Hydrol.*, 527, 668–678, <https://doi.org/10.1016/j.jhydrol.2015.05.031>, 2015.
- Hao, Z., Yuan, X., Xia, Y., Hao, F., and Singh, V. P.: An Overview of Drought Monitoring and Prediction Systems at Regional and Global Scales, *B. Am. Meteorol. Soc.*, 98, 1879–1896, <https://doi.org/10.1175/BAMS-D-15-00149.1>, 2017.
- Hersbach, H., Bell, B., Berrisford, P., Hirahara, S., Horányi, A., Muñoz-Sabater, J., Nicolas, J., Peubey, C., Radu, R., Schepers, D., Simmons, A., Soci, C., Abdalla, S., Abellan, X., Balsamo, G., Bechtold, P., Biavati, G., Bidlot, J., Bonavita, M., De Chiara, G., Dahlgren, P., Dee, D., Diamantakis, M., Dragani, R., Flemming, J., Forbes, R., Fuentes, M., Geer, A., Haimberger, L., Healy, S., Hogan, R. J., Hólm, E., Janisková, M., Keeley, S., Laloyaux, P., Lopez, P., Lupu, C., Radnoti, G., De Rosnay, P., Rozum, I., Vamborg, F., Villaume, S., and Thépaut, J.: The ERA5 global reanalysis, *Q. J. Roy. Meteor. Soc.*, 146, 1999–2049, <https://doi.org/10.1002/qj.3803>, 2020.
- Hoerling, M., Eischeid, J., Kumar, A., Leung, R., Mariotti, A., Mo, K., Schubert, S., and Seager, R.: Causes and Predictability of the 2012 Great Plains Drought, *B. Am. Meteorol. Soc.*, 95, 269–282, <https://doi.org/10.1175/BAMS-D-13-00055.1>, 2014.
- Hou, W., Chen, Z.-Q., Zuo, D.-D., and Feng, G.: Drought loss assessment model for southwest China based on a hyperbolic tangent function, *Int. J. Disast. Risk Re.*, 33, 477–484, <https://doi.org/10.1016/j.ijdr.2018.01.017>, 2019.
- Jonkman, S. N., Vrijling, J. K., and Vrouwenvelder, A. C. W. M.: Methods for the estimation of loss of life due to floods: a literature review and a proposal for a new method, *Nat. Hazards*, 46, 353–389, <https://doi.org/10.1007/s11069-008-9227-5>, 2008.
- Kucharavy, D. and De Guio, R.: Application of S-shaped curves, *Procedia Engineer.*, 9, 559–572, <https://doi.org/10.1016/j.proeng.2011.03.142>, 2011.
- Liu, R., Yin, J., Slater, L., Kang, S., Yang, Y., Liu, P., Guo, J., Gu, X., Zhang, X., and Volchak, A.: Machine-learning-constrained projection of bivariate hydrological drought magnitudes and socioeconomic risks over China, *Hydrol. Earth Syst. Sci.*, 28, 3305–3326, <https://doi.org/10.5194/hess-28-3305-2024>, 2024.
- Long, D., Yang, W., Scanlon, B. R., Zhao, J., Liu, D., Burek, P., Pan, Y., You, L., and Wada, Y.: South-to-North Water Diversion stabilizing Beijing’s groundwater levels, *Nat. Commun.*, 11, 3665, <https://doi.org/10.1038/s41467-020-17428-6>, 2020.
- Lü, J., Ju, J., Ren, J., and Gan, W.: The influence of the Madden-Julian Oscillation activity anomalies on Yunnan’s extreme drought of 2009–2010, *Sci. China Earth Sci.*, 55, 98–112, <https://doi.org/10.1007/s11430-011-4348-1>, 2012.
- Ma, M., Qu, Y., Lyu, J., Zhang, X., Su, Z., Gao, H., Yang, X., Chen, X., Jiang, T., Zhang, J., Shen, M., and Wang, Z.: The 2022 extreme drought in the Yangtze River Basin: Characteristics, causes and response strategies, *River*, 1, 162–171, <https://doi.org/10.1002/rvr2.23>, 2022.
- Mishra, A. K. and Singh, V. P.: A review of drought concepts, *J. Hydrol.*, 391, 202–216, <https://doi.org/10.1016/j.jhydrol.2010.07.012>, 2010.
- Montanari, A., Nguyen, H., Rubinetti, S., Ceola, S., Galelli, S., Rubino, A., and Zanchettin, D.: Why the 2022 Po River drought is the worst in the past two centuries, *Sci. Adv.*, 9, eadg8304, <https://doi.org/10.1126/sciadv.adg8304>, 2023.
- Neath, A. A. and Cavanaugh, J. E.: The Bayesian information criterion: background, derivation, and applications, *WIREs Computational Stats*, 4, 199–203, <https://doi.org/10.1002/wics.199>, 2012.
- Pradhan, R. K., Markonis, Y., Vargas Godoy, M. R., Villalba-Pradas, A., Andreadis, K. M., Nikolopoulos, E. I., Papalexiou, S. M., Rahim, A., Tapiador, F. J., and Hanel, M.: Review of GPM IMERG performance: A global perspective, *Remote Sens. Environ.*, 268, 112754, <https://doi.org/10.1016/j.rse.2021.112754>, 2022.
- Qiu, M., Ratledge, N., Azevedo, I. M. L., Diffenbaugh, N. S., and Burke, M.: Drought impacts on the electricity system, emissions, and air quality in the western United States, *P. Natl. Acad. Sci. USA*, 120, e2300395120, <https://doi.org/10.1073/pnas.2300395120>, 2023.
- Shao, Q., Liu, X., and Zhao, W.: An alternative method for analyzing dimensional interactions of urban carrying capacity: Case study of Guangdong-Hong Kong-Macao

- Greater Bay Area, *J. Environ. Manage.*, 273, 111064, <https://doi.org/10.1016/j.jenvman.2020.111064>, 2020.
- Shi, W., Huang, S., Liu, D., Huang, Q., Han, Z., Leng, G., Wang, H., Liang, H., Li, P., and Wei, X.: Drought-flood abrupt alternation dynamics and their potential driving forces in a changing environment, *J. Hydrol.*, 597, 126179, <https://doi.org/10.1016/j.jhydrol.2021.126179>, 2021.
- Su, B., Huang, J., Fischer, T., Wang, Y., Kundzewicz, Z. W., Zhai, J., Sun, H., Wang, A., Zeng, X., Wang, G., Tao, H., Gemmer, M., Li, X., and Jiang, T.: Drought losses in China might double between the 1.5 °C and 2.0 °C warming, *P. Natl. Acad. Sci. USA*, 115, 10600–10605, <https://doi.org/10.1073/pnas.1802129115>, 2018.
- Sun, S., Zhou, X., Liu, H., Jiang, Y., Zhou, H., Zhang, C., and Fu, G.: Unraveling the effect of inter-basin water transfer on reducing water scarcity and its inequality in China, *Water Res.*, 194, 116931, <https://doi.org/10.1016/j.watres.2021.116931>, 2021.
- Todisco, F., Mannocchi, F., and Vergni, L.: Severity–duration–frequency curves in the mitigation of drought impact: an agricultural case study, *Nat. Hazards*, 65, 1863–1881, <https://doi.org/10.1007/s11069-012-0446-4>, 2013.
- Tsoularis, A. and Wallace, J.: Analysis of logistic growth models, *Math. Biosci.*, 179, 21–55, [https://doi.org/10.1016/S0025-5564\(02\)00096-2](https://doi.org/10.1016/S0025-5564(02)00096-2), 2002.
- Van Dijk, A. I. J. M., Beck, H. E., Crosbie, R. S., De Jeu, R. A. M., Liu, Y. Y., Podger, G. M., Timbal, B., and Viney, N. R.: The Millennium Drought in southeast Australia (2001–2009): Natural and human causes and implications for water resources, ecosystems, economy, and society, *Water Resour. Res.*, 49, 1040–1057, <https://doi.org/10.1002/wrcr.20123>, 2013.
- Virtanen, P., Gommers, R., Oliphant, T. E., Haberland, M., Reddy, T., Cournapeau, D., Burovski, E., Peterson, P., Weckesser, W., Bright, J., Van Der Walt, S. J., Brett, M., Wilson, J., Millman, K. J., Mayorov, N., Nelson, A. R. J., Jones, E., Kern, R., Larson, E., Carey, C. J., Polat, İ., Feng, Y., Moore, E. W., VanderPlas, J., Laxalde, D., Perktold, J., Cimrman, R., Henriksen, I., Quintero, E. A., Harris, C. R., Archibald, A. M., Ribeiro, A. H., Pedregosa, F., Van Mulbregt, P., and SciPy 1.0 Contributors: SciPy 1.0: fundamental algorithms for scientific computing in Python, *Nat. Meth.*, 17, 261–272, <https://doi.org/10.1038/s41592-019-0686-2>, 2020.
- Wan, L., Zhou, J., Guo, H., Cui, M., and Liu, Y.: Trend of water resource amount, drought frequency, and agricultural exposure to water stresses in the karst regions of South China, *Nat. Hazards*, 80, 23–42, <https://doi.org/10.1007/s11069-015-1954-9>, 2016.
- Wang, F., Lai, H., Li, Y., Feng, K., Tian, Q., Zhang, Z., Di, D., and Yang, H.: Terrestrial ecological drought dynamics and its response to atmospheric circulation factors in the North China Plain, *Atmos. Res.*, 294, 106944, <https://doi.org/10.1016/j.atmosres.2023.106944>, 2023a.
- Wang, Y., Wang, S., Chen, Y., Wang, F., Liu, Y., and Zhao, W.: Anthropogenic drought in the Yellow River basin: Multifaceted and weakening connections between meteorological and hydrological droughts, *J. Hydrol.*, 619, 129273, <https://doi.org/10.1016/j.jhydrol.2023.129273>, 2023b.
- Wells, N., Goddard, S., and Hayes, M. J.: A self-calibrating palmer drought severity index, *J. Climate*, 17, 2335–2351, [https://doi.org/10.1175/1520-0442\(2004\)017<2335:ASPDISI>2.0.CO;2](https://doi.org/10.1175/1520-0442(2004)017<2335:ASPDISI>2.0.CO;2), 2004.
- Weng, P., Tian, Y., Zhou, H., Zheng, Y., and Jiang, Y.: Saltwater intrusion early warning in Pearl river Delta based on the temporal clustering method, *J. Environ. Manage.*, 349, 119443, <https://doi.org/10.1016/j.jenvman.2023.119443>, 2024.
- West, H., Quinn, N., and Horswell, M.: Remote sensing for drought monitoring & impact assessment: Progress, past challenges and future opportunities, *Remote Sens. Environ.*, 232, 111291, <https://doi.org/10.1016/j.rse.2019.111291>, 2019.
- Wu, Z., Li, J., He, J., and Jiang, Z.: Occurrence of droughts and floods during the normal summer monsoons in the mid- and lower reaches of the Yangtze River, *Geophys. Res. Lett.*, 33, L05813, <https://doi.org/10.1029/2005GL024487>, 2006.
- Xiong, L., Du, T., Xu, C.-Y., Guo, S., Jiang, C., and Gippel, C. J.: Non-Stationary Annual Maximum Flood Frequency Analysis Using the Norming Constants Method to Consider Non-Stationarity in the Annual Daily Flow Series, *Water Resour. Manage.*, 29, 3615–3633, <https://doi.org/10.1007/s11269-015-1019-6>, 2015.
- Yang, X., Wu, F., Yuan, S., Ren, L., Sheffield, J., Fang, X., Jiang, S., and Liu, Y.: Quantifying the Impact of Human Activities on Hydrological Drought and Drought Propagation in China Using the PCR-GLOBWB v2.0 Model, *Water Resour. Res.*, 60, e2023WR035443, <https://doi.org/10.1029/2023WR035443>, 2024.
- Ye, L., Hanson, L. S., Ding, P., Wang, D., and Vogel, R. M.: The probability distribution of daily precipitation at the point and catchment scales in the United States, *Hydrol. Earth Syst. Sci.*, 22, 6519–6531, <https://doi.org/10.5194/hess-22-6519-2018>, 2018.
- Yin, J., Slater, L., Gu, L., Liao, Z., Guo, S., and Gentile, P.: Global Increases in Lethal Compound Heat Stress: Hydrological Drought Hazards Under Climate Change, *Geophys. Res. Lett.*, 49, e2022GL100880, <https://doi.org/10.1029/2022GL100880>, 2022a.
- Yin, J., Guo, S., Yang, Y., Chen, J., Gu, L., Wang, J., He, S., Wu, B., and Xiong, J.: Projection of droughts and their socioeconomic exposures based on terrestrial water storage anomaly over China, *Sci. China Earth Sci.*, 65, 1772–1787, <https://doi.org/10.1007/s11430-021-9927-x>, 2022b.
- Yuan, X., Wang, Y., Ji, P., Wu, P., Sheffield, J., and Otkin, J. A.: A global transition to flash droughts under climate change, *Science*, 380, 187–191, <https://doi.org/10.1126/science.abn6301>, 2023.
- Zhang, L., Yuan, F., and He, X.: Probabilistic Assessment of Global Drought Recovery and Its Response to Precipitation Changes, *Geophys. Res. Lett.*, 51, e2023GL106067, <https://doi.org/10.1029/2023GL106067>, 2024.
- Zhang, X., Hao, Z., Singh, V. P., Zhang, Y., Feng, S., Xu, Y., and Hao, F.: Drought propagation under global warming: Characteristics, approaches, processes, and controlling factors, *Sci. Total Environ.*, 838, 156021, <https://doi.org/10.1016/j.scitotenv.2022.156021>, 2022.
- Zhang, Y., Keenan, T. F., and Zhou, S.: Exacerbated drought impacts on global ecosystems due to structural overshoot, *Nat. Ecol. Evol.*, 5, 1490–1498, <https://doi.org/10.1038/s41559-021-01551-8>, 2021.
- Zhao, T., Chen, Z., Tian, Y., Zhang, B., Li, Y., and Chen, X.: A decomposition approach to evaluating the local performance of global streamflow reanalysis, *Hydrol. Earth Syst. Sci.*, 28, 3597–3611, <https://doi.org/10.5194/hess-28-3597-2024>, 2024a.

Zhao, T., Li, X., Li, Y., Zhang, B., and Zhang, Y.: Concurrent droughts across Major River Basins of the World modulated by El Niño–Southern Oscillation, *J. Hydrol.*, 644, 132112, <https://doi.org/10.1016/j.jhydrol.2024.132112>, 2024b.